# Ultrasonic Nondiffracting Transducer for Medical Imaging

JIAN-YU LU, MEMBER, IEEE, AND JAMES F. GREENLEAF, FELLOW, IEEE

*Abstract*—**Historically, transducers having Gaussian shading and Fresnel shaped voltage drives on an array of annular elements have been used for medical imaging of the highest quality. These transducers have good focus within the depth of field and smooth near field patterns. Outside of the depth of field the focus degrades with diffraction effects. Nondiffracting solutions to the wave equation governing propagation in tissues (the scalar Helmholtz equation) have recently been discovered and extensively tested on electromagnetic waves. Very little work has been done with nondiffracting beams in acoustics and none in medical imaging. A study of these methods for medical imaging is reported. Computer simulations and experimental results for a ten-ring annular Bessel shaded transducer are described. Both CW and pulse wave results are shown and compared to conventional Gaussian beams. The nondiffracting beam has about 1.27-mm radius main lobe with a 20-cm depth of field compared to the Gaussian transducer of the same size with a 1.27-mm radius main lobe at a focus of 12 cm and 2 · 4-cm depth of field. The side lobes of the nondiffracting beam are the same as the $J_0$ Bessel function. The new beam forming method may have promise in novel imaging and tissue characterization modes whereby the effects of diffraction are eliminated.**

## I. Introduction

CONVENTIONALLY, transducers with Gaussian beam shading are used in medical imaging because the beam patterns are smoother in both near and far fields [1]. The Gaussian beam diverges dramatically after the Rayleigh distance because of diffraction. Dynamic focusing is used to improve lateral resolution of the Gaussian beam transducer in pulse–echo imaging. However, the transducer can be focused only at one point in transmit. The transmit beams diverge from the focal point reducing resolution. The use of a transmit beam that does not diverge throughout the region of interest would greatly improve current medical imaging methods.

Durnin [2] discovered recently a nondiffracting beam that can have long depth of field. Compared to the Gaussian beam, the nondiffracting beam has a small center lobe and relatively large side lobes that travel in parallel with the center lobe. Since the nondiffracting beam was discovered, experiments for physical realization of finite aperture $J_0$ Bessel nondiffracting beams in optics have been performed [3], [4] by J. Durnin *et al.* Several investigators have further developed the idea either in theory or experiments [5]–[10]. Only two have reported investigations of the nondiffracting beam with acoustical waves: Hsu *et al.* [11] who have constructed a Bessel beam ultrasonic transducer and Ziolkowski *et al.* [12] who have simulated an acoustic pulse wave using superposition but did not use the entire array simultaneously. These studies were very preliminary. The practical embodiment of this device for medical imaging will have advantages and disadvantages.

In this paper we report on evaluations of the nondiffracting $J_0$ Bessel beam and suggest its application to medical imaging. We report results for both computer simulations and their experimental verification with images of fields of the nondiffracting transducer for both continuous-wave (CW) and pulse-wave (PW) excitations. We also report measurements of focused and unfocused Gaussian beams produced by the same transducer for the purpose of comparisons. The effects of heterogeneity due to tissue on the nondiffracting beam and on the focused Gaussian beam are also reported.

### A. Theory

From the source-free scalar wave equation

$$\left(\nabla^2 - \frac{1}{c^2}\frac{\partial^2}{\partial t^2}\right) U(\vec{r}, t) = 0, \tag{1}$$

one can obtain the following nondiffracting solution [2]

$$U(\vec{r}, t) = e^{j(\beta z - wt)} \left| \int_0^{2\pi} A(\phi) \exp\left[-j\alpha(x\cos\phi + y\sin\phi)\right] d\phi \right|, \tag{2}$$

where

$$\begin{cases} \alpha^2 + \beta^2 = k^2, \quad k = \dfrac{w}{c} \\ 0 < \alpha \leq k. \end{cases} \tag{3}$$

where $A(\phi)$ is an arbitrary complex function of $\phi$, $\phi$ is the integration variable, $\beta$ is real, $U(\vec{r}, t)$ is sound pressure, $\vec{r} = (x, y, z)$ represents the observing point, $t$ is time, $w$ is angular frequency, and $c$ is the sound speed.

If $A(\phi)$ is independent of $\phi$, one obtains the simplest axially symmeric nondiffracting solution which is propor-

Manuscript received December 28, 1989; revised and accepted April 4, 1990. This work was supported in part by grant CA-43920 from the National Institutes of Health.

The authors are with the Biodynamics Research Unit, Mayo Clinic, 200 First Street SW, Rochester, MN 55905.

IEEE Log Number 9036915.

TABLE I
POSITIONS OF THE EDGES OF ANNULAR ELEMENTS OF THE NONDIFFRACTING ANNULAR ARRAY TRANSDUCER ALONG RADIUS

| Element # | 1 | 2 | 3 | 4 | 5 | 6 | 7 | 8 | 9 | 10 |
|---|---|---|---|---|---|---|---|---|---|---|
| Separation Positions (mm) | 2.00 | 4.59 | 7.20 | 9.81 | 12.4 | 15.0 | 17.6 | 20.3 | 22.9 | 25.0 |

tional to

$$U(\vec{r}, t) = J_o(\alpha\rho)\, e^{j(\beta z - wt)}, \tag{4}$$

where $J_o$ is the zeroth order Bessel function of the first kind and $\rho = \sqrt{x^2 + y^2}$ is the distance away from the center axis of the transducer. From (4), it is seen that the beam pattern of the $J_o$ Bessel nondiffracting solution is independent of distance, $z$, and $\alpha$ is a scaling parameter of the $J_o$ Bessel function. This means that the $J_o$ Bessel beam will travel to infinity without spreading.

### B. Practical Depth of Field

In practical applications however, only a finite aperture can be used to approximate the theoretical results of (4). In this case, the maximum nondiffracting distance of the $J_o$ Bessel beam (defined by [2, Fig. 6]) is,

$$Bz_{\max} = a\sqrt{(k/\alpha)^2 - 1}, \tag{5}$$

where $a$ is the radius of the transducer.

For an unfocused Gaussian beam generated by a finite aperture transducer, the depth of field is the Rayleigh distance which is the distance corresponding to the last maximum of the field on the center axis of the transducer. If full width at half maximum (FWHM) of the Gaussian beam at the transducer surface is $a = 25$ mm, the depth of field is given by (see appendix)

$$Gz_{\max} \approx 721 \text{ mm}. \tag{6}$$

If the Gaussian beam is focused, the depth of field $GFz_{\max}$ is defined as the distance between the two out of focus planes at which the beam spreads to $\sqrt{2}$ times the beam width in the focal plane, so (see appendix)

$$GFz_{\max} \approx \frac{2\sqrt{\frac{\sigma^4}{F^2} - \left[\left(\frac{2}{k\sigma}\right)^2 + \left(\frac{\sigma}{F}\right)^2\right]\left[\sigma^2 - 8\left(\frac{F}{k\sigma}\right)^2\right]}}{\left(\frac{2}{k\sigma}\right)^2 + \left(\frac{\sigma}{F}\right)^2}, \tag{7}$$

where $\sigma$ is the parameter of the Gaussian function $e^{-\rho^2/\sigma^2}$ at the transducer surface, and $F$ is the focal length of the lens. If the FWHM of the Gaussian beam at the transducer surface is 25 mm, $F = 120$ mm, and $k = 10.5$ mm$^{-1}$, one obtains $GFz_{\max} = 24.4$ mm. Equation (7) is valid for $\sigma^2 \ll a^2$ and $F^2 \gg \sigma^2$.

### C. Lateral Resolution

The lateral resolution of the $J_o$ Bessel nondiffracting beam is defined as the FWHM of the center lobe of the $J_o$ Bessel beam:

$$BR_L \approx \frac{3.04}{\alpha}. \tag{8}$$

If $\alpha = 1.202$ mm$^{-1}$, one obtains $BR_L \approx 2.53$ mm. Similarly the lateral resolution of the focused Gaussian beam at the focal plane is defined as the FWHM of the beam in the focal plane, which is given by (see appendix):

$$GR_L \approx 3.33\frac{F}{k\sigma}. \tag{9}$$

This equation is valid for $\sigma^2 \ll a^2$ and $F^2 \gg \sigma^2$. If FWHM = 25 mm at the transducer surface, $k = 10.5$ mm$^{-1}$ and $F = 120$ mm, one obtains $GR_L = 2.54$ mm.

From the equations above, it is seen that the nondiffracting beam can be applied to medical diagnosis with great potential utility. The nondiffracting Bessel beam has greater side lobes but much greater depth of field than the focused Gaussian beam. Its nondiffracting properties make it a potential tool for tissue characterization because the correction for diffraction will be negligible.

## II. Design of the Nondiffracting Transducer

A nondiffracting transducer was designed by us and constructed by Echo Ultrasound[1] using PZT ceramic/polymer 1-3 composite. It is a broadband transducer (about 50% of its center frequency), having a center frequency of 2.5 MHz and is composed of ten annular elements with spacing between the elements less than 0.2 mm. The transducer is backed with low impedance and matched to water with a front matching layer. The diameter of the transducer is 50 mm. The positions of edges of the annular elements along the radius were determined from Table I, which was calculated from a Bessel function when parameter $\alpha$ in (4) was chosen as 1202.45 m$^{-1}$. From Table I it is seen that the radius of the center element of the nondiffracting transducer is 2 mm. The nondiffracting distance $Bz_{\max}$ calculated from (5) is 216 mm.

## III. Computer Simulations

Pressure fields were simulated by digital computer using an annular array having the same ring parameters as the experimental transducer. The Rayleigh–Sommerfeld [13]

[1] Echo Ultrasound Inc., Lewistown, PA 17044.

scalar formulation of diffraction is very accurate for most applications. However, because there is a double integration in this formula when calculating the radiation of the Bessel beam annular array, it is very time consuming. Therefore, in the simulations we used the Fresnel approximation [13] to reduce the double integration to single and implemented it on a Sun SPARCstation 1. Differences between the Rayleigh–Sommerfeld formulation and the Fresnel approximation were found to be negligible for field points greater than 3–4 cm away from the surface of the transducer. Because the voltage, thus pressure, was constant across each annular element of the transducer, a stepwise approximation was used for the computer simulations (for stepwise Gaussian shading, see [18]). The accuracy of the field calculations was verified by experiments described in Section IV.

CW fields of the nondiffracting transducer on center axis and field distributions at several distances away from transducer gave results similar to those previously published [2] and will not be repeated here.

Pulse waves are very important for both medical imaging and Doppler measurements. Using linear system theory [13], we calculated the radiation patterns of the experimental nondiffracting transducer using excitation with a 2.5-MHz pulse of about one and one-half periods. For comparisons, the fields for focused and unfocused Gaussian beam transducers were also calculated. Images of the analytic envelope of calculated or measured pressure waves were produced at various distances from the transducers. The simulation results, as well as experimentally measured results, will be shown in Section V.

## IV. Experiments

A block diagram of the experimental set up is shown in Fig. 1. The Polynomial Waveform Synthesizer Model 2045 was used to generate either 200 $\mu$s 2.5 MHz tone bursts or the pulses for the experiment. The signal was amplified to drive the ten elements of the annular array. By changing switches in the Ten Path Driving Circuit in Fig. 1, the Bessel drive of the transducer can be easily switched to Gaussian drive. To form a focused transducer, a plexiglas lens was attached to the surface of the transducer. For Bessel drive, alternating polarities of the driving voltages were applied for the ten successive rings, and the amplitude of each ring was adjusted accordingly to make the generated acoustic pressure equal to the maximum amplitude of the respective Bessel lobes. This resulted in a stepwise approximation to the Bessel function since the pressure across the annuli were relatively constant rather than lobe shaped like the Bessel lobes. The effect of this approximation is described later. For Gaussian drive, the ten rings were driven in the same polarity, and the generated acoustic pressures were adjusted to match a stepwise approximation of the Gaussian function. The signals were received by a 0.5-mm diameter NTR System hydrophone (Model NP-1000), digitized (at 40 MHz sampling rate) and transferred to a SUN workstation for image formation and processing. Movement of the hydrophone was controlled by computer and synchronized to the data acquisition. The wideband detector and low pass filter in Fig. 1 was replaced by an offsetting buffer amplifier for the pulse experiments.

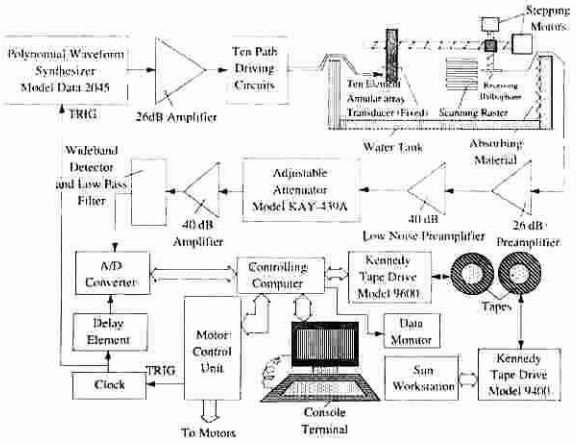


Fig. 1. Block diagram of experimental system for automatically measuring continuous and pulsed acoustic fields of Bessel and Gaussian (focused and unfocused) beam transducers.

Because of the varying properties of each element of the transducer, the acoustic field produced by each element did not have exactly the desired amplitude at a given field point even if the electrical signal on the transducer element had exact Bessel or Gaussian amplitudes. To set up the appropriate fields for each annulus, computer simulations were done for each annular element at distance $z$ = 205 mm on the central axis of the transducer. This distance was chosen to avoid rapid variation of the fields from the outer ring element. The calculated normalized amplitudes of the fields at this point ($z$ = 205 mm) for both Bessel and Gaussian beams are tabulated in Table II.

The amplifiers on each annulus were adjusted individually to produce the correct pressure as measured by the hydrophone at 205 mm on the central axis of each ring. This procedure corrected for variations in the ring responses.

## V. Results

### A. Continuous Wave Studies

Fig. 2 shows images of the computer simulated pressure field of the nondiffracting transducer for an exact CW $J_0$ Bessel drive (acoustic field profile is an exact Bessel shading function at the transducer surface). The field was calculated over a rectangular area 48 mm wide and 200 mm long through the central axis of the transducer with a pixel size of 0.48 mm × 0.5 mm. Each image begins 5 mm away from the surface of the transducer. The gray levels of the images are linear, log compressed, −6-dB clipped log compressed and −12-dB clipped log compressed, respectively, as marked. The field is virtually diffraction free for almost 20 cm.

Fig. 3(a) shows the computer simulated pressure field of the nondiffracting transducer for CW with stepped Bessel shading on the annuli. Panel (b) shows the pressures

TABLE II
ON AXIS RELATIVE FIELD PRESSURES AT 205 mm FOR STEP DRIVE BESSEL AND GAUSSIAN BEAMS

| Element # | 1 | 2 | 3 | 4 | 5 | 6 | 7 | 8 | 9 | 10 |
|---|---|---|---|---|---|---|---|---|---|---|
| Bessel Beam | 1.00 | 1.75 | 2.31 | 2.70 | 2.99 | 3.18 | 3.28 | 3.32 | 3.28 | 3.02 |
| Gaussian Beam | 1.00 | 4.13 | 6.59 | 7.85 | 7.91 | 7.01 | 5.58 | 4.03 | 2.66 | 1.61 |

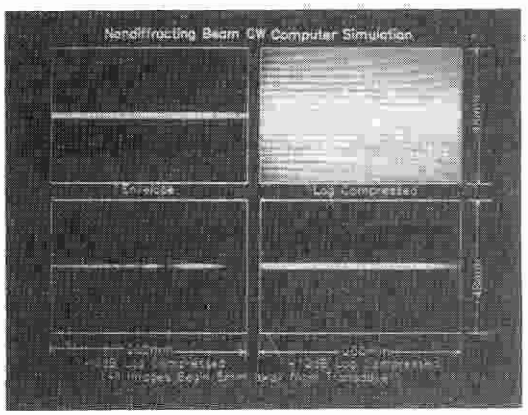


Fig. 2. Continuous wave computer simulation for exact Bessel beam nondiffracting transducer. Four images in figure are same field magnitude displayed in envelope (linear), log compressed, −6 dB clipped log compressed, and −12 dB clipped log compressed, respectively. All images begin 5 mm away from transducer and pixel size is 0.48 mm × 0.5 mm.

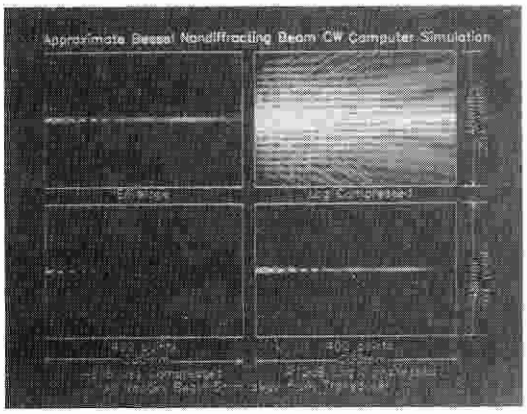


(a)

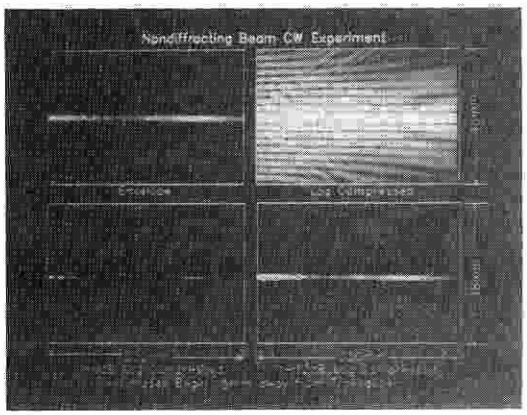


(b)

Fig. 3. Continuous-wave computer simulation (a) and experimental measurements (b) for a step Bessel approximation of nondiffracting transducer. Format is same as in Fig. 2.

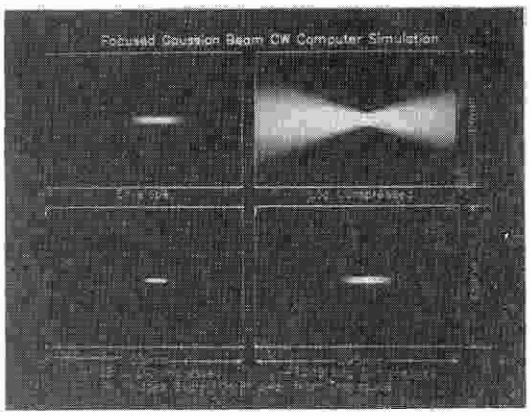


Fig. 4. Continuous wave computer simulations for exact focused Gaussian beam transducer. Focal length is 120 mm. Displays are in format of Fig. 2. All images begin 10 mm away from transducer, and pixel size is 0.48 mm × 0.5 mm.

experimentally measured using the system of Fig. 1. The effect of a step approximation of the Bessel beam is clearly predicted by the simulation.

Figs. 4 and 5 are images of computed and experimentally measured fields of the ten element annular array transducer for a CW focused Gaussian drive in the same format as Figs. 2 and 3, respectively. The focal length is 120 mm and the field dimensions are 195 mm (long) by 48 mm (wide). Each image begins 10 mm away from the surface of the transducer. The step approximation also makes a difference in this case.

### B. Pulse–Wave Studies

Figs. 6–8 illustrate simulated (with a pulse wave (PW) and exact shading (a) and step shading (b)) and experimentally measured (with a pulse wave and step shading (c)) images of −6-dB clipped log compressed pulse fields generated by nondiffracting (Fig. 6), focused Gaussian (Fig. 7) and unfocused Gaussian beam (Fig. 8) transducers. Each panel includes images at four distances ($z$ = 50 mm, 100 mm, 150 mm, and 216 mm) away from the surface of the transducers (except Fig. 7 for the case of the focused Gaussian beam whose distances were set to $z$ = 50 mm, 120 mm, 150 mm, and 216 mm). The electrical pulse used to excite the transducers for both simulations and experiments was of the form

$$f(t) = e^{-t^2/t_o^2} \sin(2\pi f_o t), \tag{10}$$

where $f_o$ = 2.5 MHz and $t_o$ = 0.4 μs. The sound speed was assumed to be $c$ = 1.5 mm/μs. The width of the

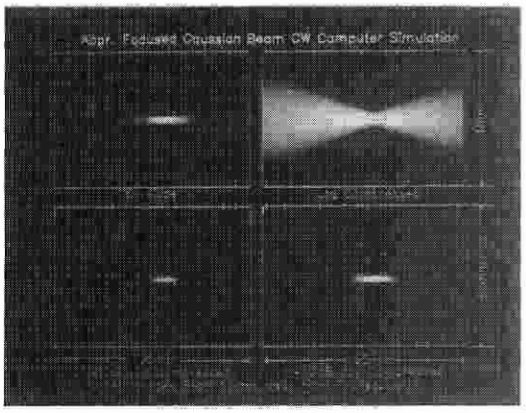


(a)

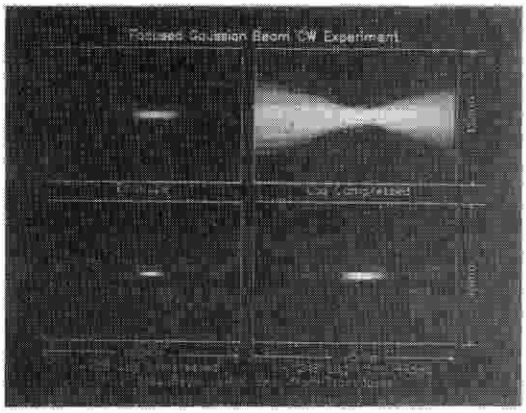


(b)

Fig. 5. Continuous wave computer simulation (a) and experiment (b) for step drive focused Gaussian beam transducer. Each panel corresponds to that in Fig. 4.

images was 50 mm (201 points) and length was 10.24 $\mu$s (256 points). The focal length of the focused Gaussian beam transducer was 120 mm and the FWHM (full width at half maximum) of the focused and unfocused shading of the Gaussian beam at the face of the transducer was 25 mm, which was the radius of the transducer. These results illustrate that for pulses little error is introduced by approximating the Bessel function shading with positive and negative steps of magnitude equal to the peak of respective lobes of the Bessel function. The Gaussian function can be approximated with a stepwise function as well. This greatly relieves constraints on transducer design.

### C. Phase Aberration by Tissue

To study the phase aberrations of the nondiffracting beam by soft biological tissue, a 10-mm layer excised beef tissue (muscle plus fat) was placed in front of the transducer. The results are shown in Figs. 9(a) (CW case) and (b) (PW case). Figs. 10(a) (CW case) and (b) (PW case) are the results of the effects of the same beef tissue on the focused Gaussian beam transducer. It is seen that the biological tissue has about the same effects on both the nondiffracting and the focused Gaussian beams.

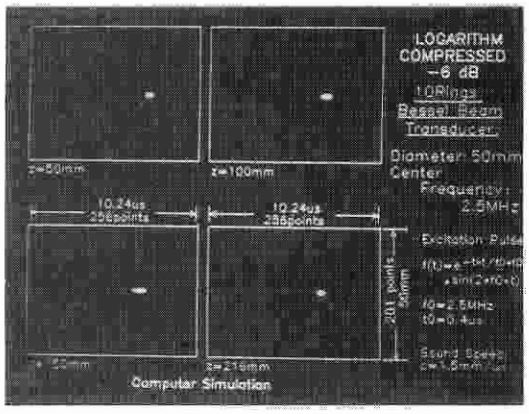


(a)

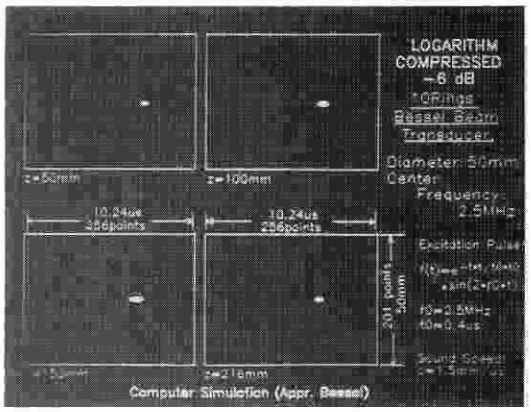


(b)

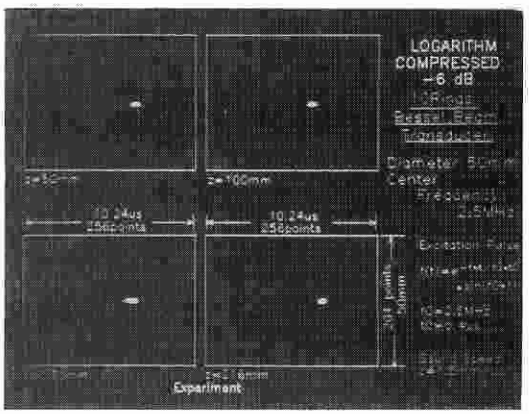


(c)

Fig. 6. Pulse wave computer simulations (with an exact drive (a) and step drive (b)) and experimental measurements (with a step drive (c)) for Bessel beam nondiffracting transducer. Images are measured at four distances: $z$ = 50 mm, 100 mm, 150 mm, and 216 mm, respectively, and pixels within −6 dB of the field maximum are log compressed and displayed. The pixel size is 0.06 mm × 0.25 mm.

## VI. Conclusion

### A. Summary

A ten-element nondiffracting annular array was fabricated using PZT ceramic/polymer 1-3 composite. The fields of this array for CW and pulsed drive were obtained by both computer simulations and experiments. Very large

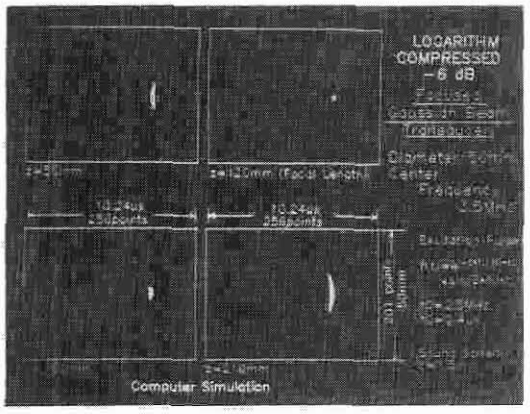


(a)

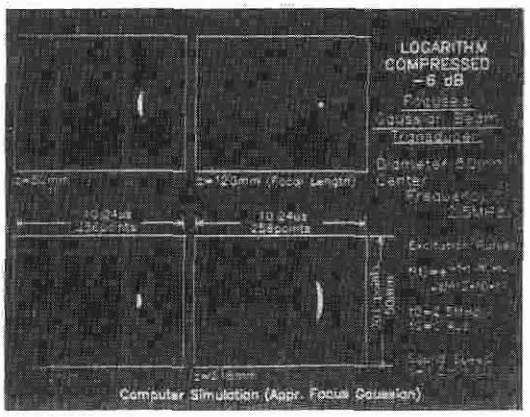


(b)

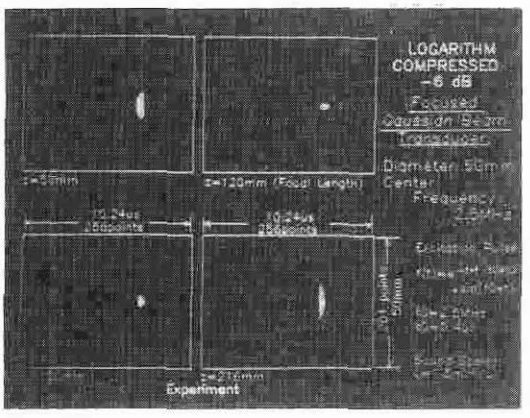


(c)

Fig. 7. Pulse-wave computer simulations (with exact drive (a) and step drive (b)) and experimental measurements (with step drive (c)) for focused Gaussian beam transducer. Focal length is 120 mm. Images are measured at four distances $z$ = 50 mm, 120 mm, 150 mm, and 216 mm, respectively, and pixels within −6 dB of the field maximum are log compressed and displayed. The pixel size is 0.06 mm × 0.25 mm.

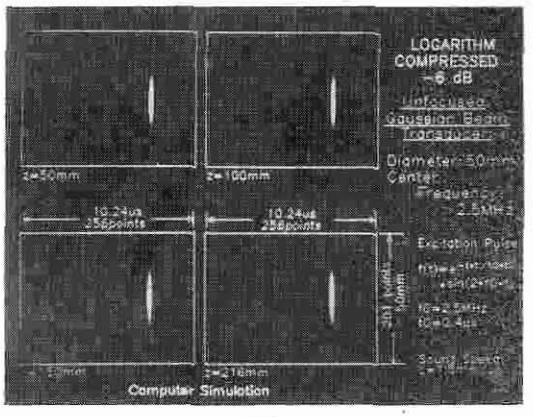


(a)

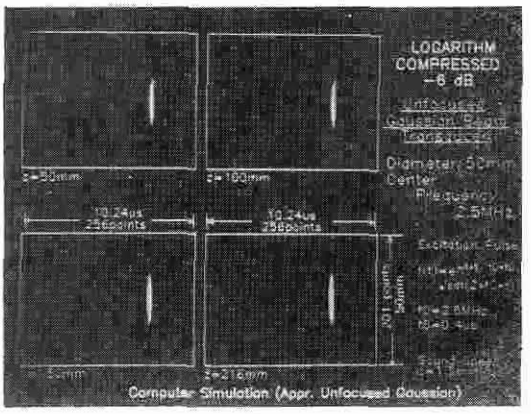


(b)

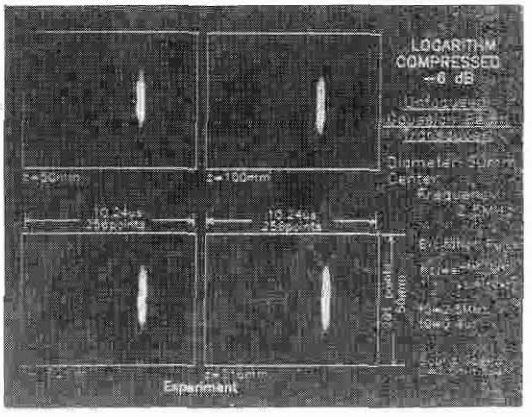


(c)

Fig. 8. Pulse-wave computer simulations (with an exact drive (a) and step drive (b)) and experimental measurements (with a step drive (c)) for unfocused Gaussian beam transducer. Images are measured at four distances $z$ = 50 mm, 100 mm, 150 mm, and 216 mm, respectively, and pixels within −6 dB of the field maximum are log compressed and displayed. Pixel size is 0.06 mm × 0.25 mm.

depth of field ( >200 mm with a transducer radius of 25 mm) was observed with the radius of the center lobe of the nondiffracting Bessel beam equal to about 1.27 mm throughout the depth of field. Good agreement between the simulations and experiments was obtained. The nondiffracting beam was also compared to conventional focused and unfocused Gaussian beams. The effects of biological tissue on both the nondiffracting and the conventional focused Gaussian beams were also tested and found to be about equal.

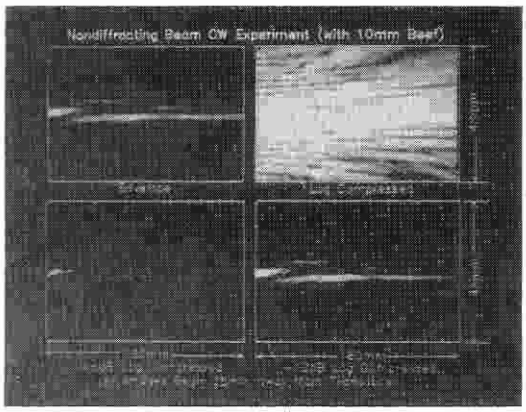


(a)

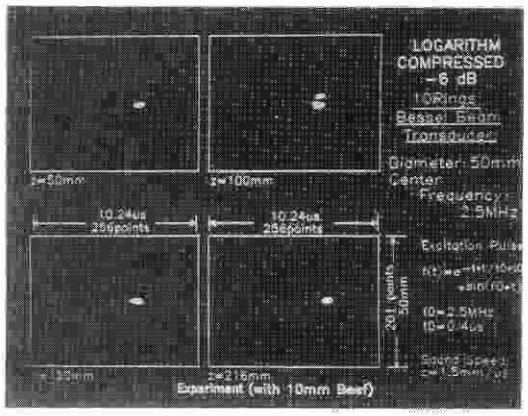


(b)

Fig. 9. Effects of 10-mm beef tissue (muscle plus fat) on continuous field (a) and pulse field (b) of step drive Bessel beam nondiffracting transducer. The beef is placed in front of the transducer. The images in (a) and (b) are measured and displayed using the same parameters as those in Figs. 3 and 6, respectively (because of the beef, the images in (a) start 25 mm away from the transducer and the size of the field is 180 mm × 48 mm, instead of 200 mm × 48 mm).

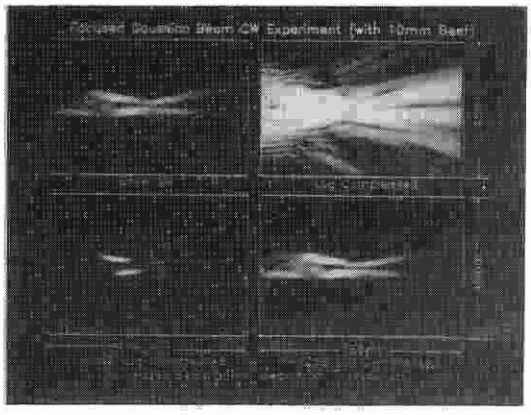

(a)

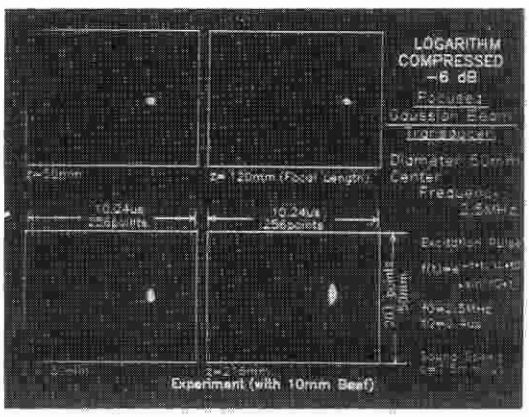


(b)

Fig. 10. The effects of 10-mm beef tissue (muscle plus fat) on continuous field (a) and pulse field (b) of step drive focused Gaussian beam transducer. Beef is placed in front of transducer. Images in (a) and (b) are measured and displayed using same parameters as those in Figs. 5 and 7, respectively (for placing beef, images in (a) start 25 mm away from transducer, and the size of field is 180 mm × 48 mm, instead of 195 mm × 48 mm).

Although the diameter of the Gaussian beam at the focus was smaller, the diameter of the beams before and after the focus were very broad compared to the nondiffracting beam.

### *B. Discussion*

Hsu *et al.* [11] constructed a three-ring, narrow band solid PZT $J_o$ Bessel nondiffracting transducer using a nonuniform poling technique. With this transducer, they generated rough CW nondiffracting fields. They did not study further the properties of this transducer in pulse mode required for medical imaging. In 1989, Ziolkowski *et al.* [12] simulated nondiffracting pulsed acoustic waves using a linear array and a square array. However, they generated the pulse waves using superposition of the contribution of each element of the transducer array (each element was excited by a complex time function) and did not use the entire array simultaneously. Also, they did not apply their method to medical imaging. In this paper, we have designed a broadband $J_o$ Bessel nondiffracting transducer fabricated by Echo Ultrasound using PZT ceramic/polymer 1–3 composite. Because the $J_o$ Bessel profile is symmetric and the amplitudes of the lobes can be approximated with step functions (see Section IV in this paper), it is easily constructed. With this nondiffracting annular array transducer, we have successfully generated both CW and pulsed waves that were not greatly distorted by the phase aberrating effects of biological tissue. The advantages of composites (high electromechanical coupling coefficient, low crosstalk between elements of array, low acoustical impedance and broad bandwidth [14]) allow this nondiffracting transducer to be applied immediately to medical imaging.

Because of the long depth of field ( $>200$ mm), the $J_o$ Bessel nondiffracting transducer could be used to replace the multiple transmits required in conventional *B*-scanners that reduce the imaging frame rate resulting in blurred im-

ages of moving objects. The small size of the center lobe of the $J_o$ Bessel nondiffracting transducer may make it possible to eliminate dynamic focusing in the receive mode in commercial imaging instruments, simplifying the designs of these instruments. $J_o$ Bessel nondiffracting transducers could also be used in transmission imaging, such as transmission ultrasonic tomography with the expectation of obtaining higher imaging quality over the conventional Gaussian beam transducer which must be focused at a fixed distance. Another potential application of the $J_o$ Bessel nondiffracting transducer would be tissue characterization which requires correction for diffraction for the estimation of tissue attenuation or $B/A$ (nonlinear parameter) [15]–[17].

The $J_o$ Bessel function determines the amplitude of the side lobes of the nondiffracting beam. These side lobes could be reduced in the pulse echo mode if a $J_o$ Bessel nondiffracting receiver is used because the transmit and receive beams are multiplied with one another. In pulse-echo imaging, dynamic focusing in receiving could also be considered to further suppress the side lobes. From (5), it is seen that the size of the transducer, $a$, the maximum nondiffracting distance, $Bz_{\max}$, and $\alpha$ which determines the width of the center lobe of the Bessel beam, trade off with each other. If $Bz_{\max}$ is fixed, to reduce the size of the center lobe of the $J_o$ Bessel beam ($\alpha$ increase), the size of the transducer, $a$, should be increased. Similarly, if $a$ is fixed, $Bz_{\max}$ will reduce when the size of the center lobe of the beam decreases. These tradeoffs are similar to those of the Gaussian transducer in which depth of field and resolution are related. Effective use of the nondiffracting transducer in medical imaging will require complete understanding of the effects of these tradeoffs on resolution, speckle, and contrast.

## Appendix
## Derivation of Lateral Resolution and Depth of Field of Focused and Unfocused Gaussian Beam Transducer

From the Fresnel approximation [13], one obtains the field of a transducer shaded by a circularly symmetric function $A(\rho)$:

$$U(P_o) = \frac{kze^{jk\sqrt{x_o^2+z^2}}}{j(x_o^2+z^2)} \int_0^a A(\rho) J_o\left(-\frac{kx_o\rho}{\sqrt{x_o^2+z^2}}\right) \cdot \exp\left[jk\rho^2/(2\sqrt{x_o^2+z^2})\right]\rho\, d\rho, \quad (11)$$

where $P_o = (x_o, z)$ is an observation point, $\rho = \sqrt{x^2+y^2}$ is the distance away from the center axis of the transducer, $J_o$ is the zeroth-order Bessel function of the first kind, $k = 2\pi/\lambda$ is wave number and $\lambda$ is wavelength.

Let $A(\rho)$ be the shading of focused Gaussian transducer, i.e.,

$$A(\rho) = e^{-\rho^2/\sigma^2} \exp\left[-jk(\sqrt{F^2+\rho^2} - F)\right], \quad (12)$$

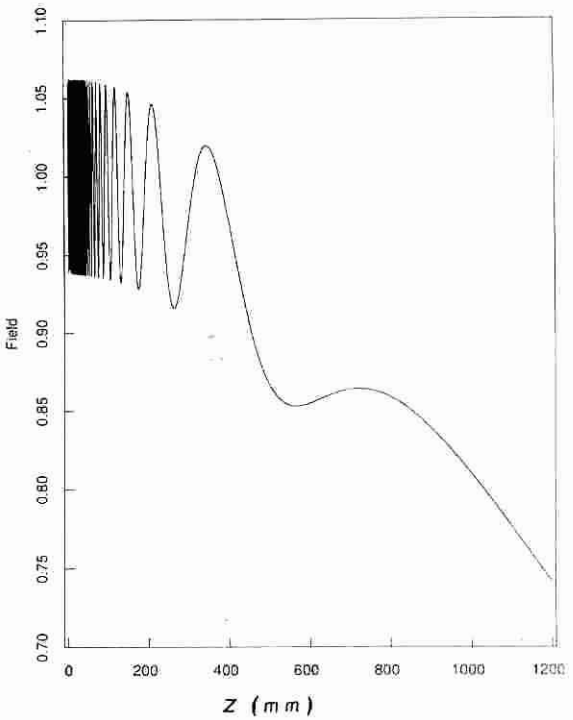


Fig. 11. Field of unfocused beam transducer on center axis.

where $F$ is the focal length of the lens and $\sigma$ is the $1/e$ radius of the Gaussian beam on the transducer surface.

### A. Field of Unfocused Transducer on Center Axis

For an unfocused transducer, the shading is of the form

$$A(\rho) = e^{-\rho^2/\sigma^2}, \ (F \to \infty). \quad (13)$$

For the field on center axis ($x_o = 0$), (11) can be integrated

$$\left|U(z)\right| = \frac{ke^{-a^2/\sigma^2}}{\sqrt{k^2 + 4\dfrac{z^2}{\sigma^4}}} \cdot \sqrt{1 + e^{2a^2/\sigma^2} - 2e^{a^2/\sigma^2}\cos ka^2/2z}. \quad (14)$$

Equation (14) is plotted in Fig. 11 where $\sigma = 15$ mm (FWHM = 25 mm), $a = 25$ mm, and $k = 10.5$ mm$^{-1}$.

### B. Depth of Field of Unfocused Gaussian Beam Transducer

If we define the depth of field of an unfocused Gaussian beam transducer as $Gz_{\max}$ that corresponds to the last maximum of the field on the center axis, from Fig. 11, it is seen that

$$Gz_{\max} \approx 721 \text{ mm}. \quad (15)$$

This is (6) in the paper.

### C. Lateral Resolution of Focused Gaussian Beam at Focal Plane

Substitute (12) into (11), we have

$$U(P_o) = \frac{kze^{jk\sqrt{x_o^2+z^2}}}{j(x_o^2+z^2)} \int_0^a \exp\left[-\rho^2/\sigma^2 - jk(\sqrt{F^2+\rho^2}-F)\right] J_o\left(-\frac{kx_o\rho}{\sqrt{x_o^2+z^2}}\right) \cdot \exp\left[jk\rho^2/(2\sqrt{x_o^2+z^2})\right]\rho\, d\rho. \quad (16)$$

If $F^2 >> \sigma^2$, one has

$$\sqrt{F^2+\rho^2} - F \approx \rho^2/2F \quad (17)$$

and if $\sigma^2 << a^2$, the upper limit of the integration in (15) can be approximated by $\infty$. Using

$$\int_0^\infty x e^{-Px^2} J_o(\xi x)\, dx = \frac{1}{2P} e^{-\xi^2/4P}, \quad (18)$$

where $P$ and $\xi$ are parameters which are independent of $x$, (16) can be written as

$$\left|U(P_o)\right| \approx \frac{kz}{2(x_o^2+z^2)} \cdot \frac{1}{\sqrt{\frac{1}{\sigma^4} + k^2\left(\frac{1}{2F} - \frac{1}{2\sqrt{x_o^2+z^2}}\right)^2}} \cdot \exp\left\{-\left[\frac{k^2x_o^2}{(x_o^2+z^2)\sigma^2}\right] \Big/ \left[4\left(\frac{1}{\sigma^4} + k^2\left(\frac{1}{2F} - \frac{1}{2\sqrt{x_o^2+z^2}}\right)^2\right)\right]\right\}. \quad (19)$$

The lateral resolution of the focused Gaussian beam transducer can be defined as the FWHM of the transverse profile of the beam at distance $z$, and it can be obtained from (19) (assume $z >> x_o$)

$$R_L(z) = 2\sqrt{-(\ln 0.5)\left[\left(\frac{2z}{k\sigma}\right)^2 + \left(\frac{\sigma}{F}\right)^2 (z-F)^2\right]}. \quad (20)$$

At focal plane ($z = F$), the lateral resolution is given by

$$GR_L \approx 3.33\frac{F}{k\sigma}, \quad (21)$$

which is the derivation of (9).

### D. Depth of Field of Focused Gaussian Beam Transducer

If we define the depth of field of the focused Gaussian beam transducer as the distance between two out of focus planes in which the beam spreads to $\sqrt{2}$ times the beam width in the focal plane, from (20), the depth of field can be obtained

$$GFz_{\max} \approx 2\frac{\sqrt{\frac{\sigma^4}{F^2} - \left[\left(\frac{2}{k\sigma}\right)^2 + \left(\frac{\sigma}{F}\right)^2\right]\left[\sigma^2 - 8\left(\frac{F}{k\sigma}\right)^2\right]}}{\left(\frac{2}{k\sigma}\right)^2 + \left(\frac{\sigma}{F}\right)^2}. \quad (22)$$

which is (7) in the paper.


## Acknowledgment

The authors appreciated the help of Randy Kinnick for building the driving circuits of the nondiffracting transducer. The authors are grateful for the secretarial assistance of Elaine Quarve and the graphic assistance of Christine Welch.


## References


[1] G. S. Kino, *Acoustic Waves: Devices, Imaging, and Analog Signal Processing*. Englewood Cliffs, NJ: Prentice-Hall, 1987, ch. 3.

[2] J. Durnin, "Exact solutions for nondiffracting beams. I. The scalar theory," *J. Opt. Soc. Am.*, vol. 4, no. 4, pp. 651–654, 1987.

[3] J. Durnin and J. J. Miceli, Jr., "Diffraction-free beams," *Phys. Rev. Lett.*, vol. 58, no. 15, pp. 1499–1501, 1987.

[4] J. Durnin, J. J. Miceli, Jr., and J. H. Eberly, "Experiments with nondiffracting needle beams," Optical Society of America, Washington, DC, available from IEEE Service Center (cat. No. 87CH2391-1), Piscataway, NJ, 1987, p. 208.

[5] F. Gori, G. Guattari, and C. Padovani, "Bessel-Gaussian beams," *Optics Commun.*, vol. 64, no. 6, pp. 491–495, Dec. 15, 1987.

[6] ——, "Model expansion for $J_o$-correlated Schell-model sources," *Optics Commun.*, vol. 64, no. 4, pp. 311–316, Nov. 15, 1987.

[7] K. Uehara, and H. Kikuchi, "Generation of near diffraction-free laser beams," *Appl. Physics B*, vol. 48, pp. 125–129, 1989.

[8] L. Vicari, "Truncation of nondiffracting beams," *Optics Commun.*, vol. 70, no. 4, pp. 263–266, Mar. 15, 1989.

[9] M. Zahid and M. S. Zubairy, "Directionally of partially coherent Bessel-Gauss beams," *Optics Commun.*, vol. 70, no. 5, pp. 361–364, April 1, 1989.

[10] S. Y. Cai, A. Bhattacharjee, and T. C. Marshall, " 'Diffraction-free' optical beams in inverse free electron laser accelerators," *Nuclear Instruments and Methods in Physics Research, Section A: Accelerators, Spectrometers, Detectors and Associated Equipment*, vol. 272, no. 1-2, pp. 481–484, Oct. 1988.

[11] D. K. Hsu, F. J. Margetan, and D. O. Thompson, "Bessel beam ultrasonic transducer: Fabrication method and experimental results," submitted for publication in *Appl. Phys. Lett.*, Nov. 1989.

[12] R. W. Ziolkowski, D. K. Lewis, and B. D. Cook, "Evidence of localized wave transmission," *Phys. Rev. Lett.*, Jan. 8, 1989, vol. UME62, no. 2, pp. 147–150.

[13] J. W. Goodman, *Introduction to Fourier Optics*. New York: McGraw-Hill, 1968, chs. 2-4.

[14] W. A. Smith, "The role of piezocomposites in ultrasonic transducers," *1989 IEEE Ultrason. Symp. Proc.*, Montréal, PQ, Canada, October 3-6, 1989 (in Press).

[15] M. Insana, J. Zagzebski, and E. Madsen, "Improvements in the spectral difference method for measuring ultrasonic attenuation," *Ultrason. Imaging*, 1983, vol. 5, no. 2, pp. 331–345.

[16] M. A. Fink and J. F. Cardoso, "Diffraction effects in pulse-echo measurement. *IEEE Trans. Sonics Ultrason.*, vol. SU-31, no. 4, pp. 313–329, July 1984.

[17] T. Sato, A. Fakusima, N. Ichida, H. Ishikawa, H. Miwa, Y. Igarashi, T. Shimura, and K. Mwrakami, "Nonlinear parameter tomography

system using counterpropagating probe and pump wave," *Ultrason. Imag.*, vol. 7, pp. 49–59, July 1985.

[18] R. O. Claus and P. S. Zerwekh, "Ultrasonic transducer with a two-dimensional Gaussian field profile," *IEEE Trans. Sonics Ultrason.*, vol. SU-30, no. 1, pp. 36–39, Jan. 1983.

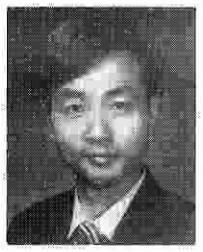

**Jian Yu Lu** (M'88) was born in Fuzhou, Fujian Province, People's Republic of China, on August 20, 1959. He received his B.S. degree from Fudan University, Shanghai, China, in 1982, the M.S. degree from Tongji University, Shanghai, China, in 1985, and the Ph.D. degree from Southeast University, Nanjing, China, in 1988.

Since December 1988, he is a postdoctoral research fellow in the Biodynamics Research Unit, Department of Physiology and Biophysics, Mayo Clinic and Foundation, Rochester, MN. His research interests are acoustical imaging, novel ultrasonic transducers for medical application, and tissue characterization.

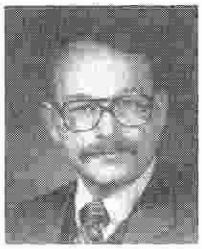

**James F. Greenleaf** (M'73–SM'84–F'88) was born in Salt Lake City, UT, on February 10, 1942. He received the B.S. degree in electrical engineering from the University of Utah, Salt Lake City, in 1964, the M.S. degree in engineering science from Purdue University, Lafayette, IN, in 1968, and the Ph.D. degree in engineering science from the Mayo Graduate School of Medicine, Rochester, MN, and Purdue University, West Lafayette, IN, in 1970.

He is currently Professor of Biophysics and Medicine, Mayo Medical School, and Consultant, Biodynamics Research Unit, Department of Physiology, Biophysics, and Cardiovascular Disease and Medicine, Mayo Foundation. He has served on the IEEE Technical Committee for the Ultrasonics Symposium for five years. He served on the IEEE-UFFCS Subcommittee on Ultrasonics in Medicine/IEEE Measurement Guide Editors, and on the IEEE Medical Ultrasound Committee.

Dr. Greenleaf is Vice President of the UFFCS Society. Dr. Greenleaf has four patents and is recipient of the 1986 J. Holmes Pioneer award from the American Institute of Ultrasound in Medicine and is a Fellow of AIUM. His special field is in ultrasonic biomedical imaging science and has published more than 146 articles and edited four books in the field.